Avizo

Effective Multimodal Multiscale Analytical and Imaging Correlation

Alexander S. Hall, Leah L. Lavery, and Pascal Doux

Materials and Structural Analysis, Thermo Fisher Scientific, Houston, TX 77084, USA

Manuscript received September 13, 2018; revised October 21, 2018; accepted October 24, 2018. Date of publication; date of current version.

Abstract—Microstructure impacts material properties such as wear resistance, ductility, toughness, conductivity, and permeability. Notably, no single microscope can examine microstructure at all length scales and with all modes of data acquisition. In these cases, multimodal multiscale microscopy integrates results from multiple devices into cohesive understanding. Three cases present hardware and software to merge image or spectral data collected by different microscopes and detectors to achieve new insights: 1) microcomputed tomography and scanning electron microscopy of a porous rock core, 2) plasma focused ion beam and energy-dispersive spectroscopy (EDS) of a shale matrix, and 3) correlative light and electron microscopy in a cryo environment. In each case, thoughtful experimental designs, integrated sample holders, accessible file formats, online software, and offline postprocessing permitted integrated investigation of microstructure in heterogeneous samples.

Index Terms—Avizo, computed tomography (CT), correlative light and electron microscopy (CLEM), PerGeos.

I. INTRODUCTION

Understanding the relationship between material properties and underlying microstructure is a major goal of disciplines like materials science and geosciences. Given that the features affecting material properties extend across many length scales, this often requires acquire data at multiple resolution levels from the same sample. The size of the microstructure will interact with its shape to generate nonlinear effects at a nanoscale, such as fluid flow through a microporous rock or metal corrosion [1]. Furthermore, electron microscopy and X-ray imaging provide additional imaging modalities for materials characterization beyond optical microscopy. Combining inferences from multiple modes of acquisition, or correlative microscopy, can also be combined with multiscale microscopy [2], thus leading to the term multimodal multiscale data. In materials science and biology, multimodal multiscale microscopy is emerging as a way to more quickly and accurately understand the nature of materials to inform their function and application to a task [2].

Imaging samples across microscopes and scales invokes a range of integration. Since the area or volume analyzed decreases with increasing resolution, it becomes necessary to accurately and quickly colocate areas of interest across microscopes. At one extreme, this would be handled manually "by eye" using the features present in the data to assume colocality across data scales. At the another end of this spectrum, a totally integrated multimodal microscope would perform synchronous specimen measurement and analysis. Features would be colocated by pairing a spatially aware sample holder and software that uses a common coordinate system across modalities. In practice, multimodal multiscale imaging typically invokes levels of integration in between these two extremes. Generally speaking, software can overcome or supplement absent hardware integration to improve integration between imaging hardware. What follows are three case studies where integrated solutions applied using microscopy hardware and image analysis software.

Corresponding author: Alexander S. Hall (e-mail: allopatry@gmail.com).
Associate Editor: A. Mueller.
Digital Object Identifier 10.1109/LSENS.2018.2878667

II. CASE STUDIES

A. Porosity Analysis of Entire Rock Core at Micrometer Resolution

Porosity must be considered to accurately account for the total retrievable volume of oil and natural gas reserves from reservoirs. Rock cores are often examined volumetrically in their entirety using traditional computed tomography (CT), but the limits of resolution in X-ray microscopy fail to resolve all microporous features [3], [4]. Thus, one can physically extract a subplug to scan in a much higher resolution micro-CT instrument. Additionally, electron microscopy can supplement the X-ray CT data to assess microporosity at the higher resolution, when necessary.

A study was performed using a Middle East carbonate sample "SD1" owned by the Masdar Institute of Science and Technology. The rock sample was 7.5 cm tall and 3.8 cm in diameter (see Fig. 1). From perfusion analyses performed in a dedicated laboratory, the reference porosity of the specimen was ascertained to be 14.4%. The goal was to determine the level of porosity in the rock sample using digital rock analysis so as to assess the validity of an upscaling workflow. To do this, 16 bit grayscale image data were acquired at three resolutions: a micro-CT scan at 16 μm^3, a microCT scan of a 10 mm diameter subplug at 5 μm^3, and a 10 mm diameter SEM slice at 2 μm^2 (see Fig. 1). The micro-CT scans were acquired using a Thermo Fisher Scientific HeliScan and the SEM data were collected using a Thermo Fisher Scientific Quanta.

Using Thermo Scientific PerGeos Software, the SEM 2-D dataset were digitally aligned to the subplug 3-D dataset and then aligned the subplug dataset to the full 3-D volume micro-CT scan (see Fig. 1). Once coregistered, the porosity determined from the 2 μm^2 SEM slice (10.56%) was extrapolated to the same 5 μm^2 micro-CT slice using adaptive thresholding. The 2 μm^2

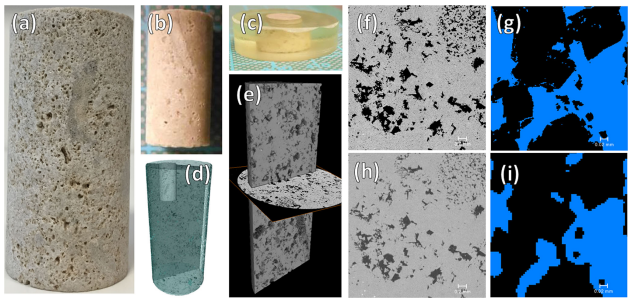

Fig. 1. Multimodal multiscale porosity analysis of a carbonate rock "SD1." The (a) initial core, (b) subplug, and (c) polished surface for SEM. The core was μCT-scanned at 16 μm^3 resolution and (d) registered to a 5 μm^3 μCT scan of the subplug. Additionally (e) the SEM slice was aligned to the subplug. At the 2 μm^2 resolution of the SEM data [(f)–(g)], microporosity was clearly visible and could be isolated. Even at 5 μm^2 resolution [(h)–(i)], such microporosity was not consistently resolved in the μCT data. By upscaling the SEM porosity inference to the subplug and then to the whole CT data, one can calculated the porosity of a large volume at the nanoscale.

resolution was high enough to let us assume that the pores were all resolved; that is, the boundary between pores and rock was clearly established. Thus, a threshold value was obtained that yielded the same porosity (10.56%) for the lower resolution micro-CT slice. This threshold value was then applied to the whole micro-CT subplug. Upscaling the SEM porosity to the micro-CT subplug yielded a porosity of 14.95%. PerGeos revealed that the total connected porosity of the subplug was 14.41%.

The authors then digitally examined the overlapping subvolume covered by the subplug in the full micro-CT dataset. Doing this again permitted applying adaptive thresholding to find the threshold value for the full micro-CT dataset that would yield the porosity determined from the micro-CT subplug (14.95%). After upscaling this threshold value to the full micro-CT dataset, a total porosity equal to 15.2% was revealed. Finally, the total connected porosity of the SD1 rock was found to be 14.6%.

Initially, the authors attempted to threshold the low-resolution micro-CT data to obtain a measure of porosity in the specimen. Due to the inability of the 16 μm^3 micro-CT data to detect microporous cracks, fissures, and holes, a top-hat direct thresholding approach yielded a too-low porosity of 10.91%. Recall that the established connected porosity as measured by perfusion was known to be 14.4%. Even the subplug, with a 5 μm^3 resolution, could only recover 11.03% connected porosity (11.27% total porosity). In this case, it was necessary to include higher resolution electron microscopy data. Coregistering SEM data with two micro-CT datasets allowed for an accurate, digital reconstruction of connected porosity in this carbonate rock. See the following videos demonstrating the multiscale visualization and upscaling workflow: 1) https://www.youtube.com/watch?v = pY6kJGJk6tY; 2) https://www.youtube.com/watch?v = v4ayOecFCVc. Overall, this first case demonstrated a multiscale multimodal (μCT and SEM) analysis to verify a digital rock analysis workflow.

B. Plasma FIB Multimodal Shale Porosity Analysis

When microporosity in heterogeneous samples remains below the resolution limits of CT, plasma focused ion beam (PFIB) presents an alternative. Compared to focused ion beam (FIB) milling with a Ga^+ or

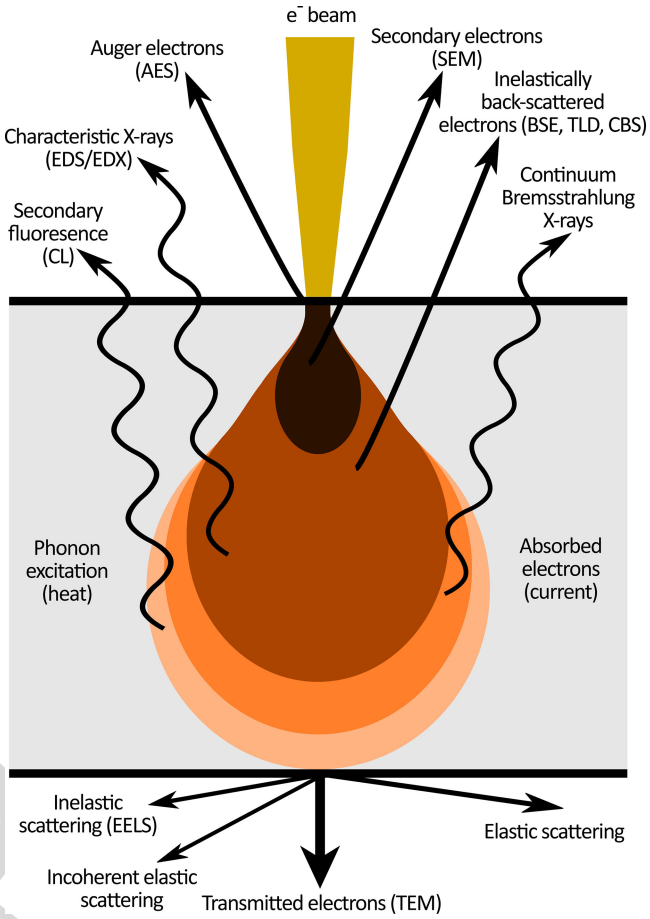

Fig. 2. Summary of the electron interaction volume. Useful radiation and particles are emitted when materials are interrogated with an electron beam. The emitted radiation and particles are the signal source for several modalities, as shown. Modified from original image by Wikimedia Commons user Claudionico, distributed under a CC BY-SA 4.0 license.

He^+ source, PFIB with an Xe^+ source can mill larger volumes with less energy [5], [6]. PFIB, like FIB–SEM, provides exceptionally resolved 3-D imagery from a serial stack of milled slices. As seen in Fig. 2, electron microscopes work by passing electrons through a material, thus producing an electron interaction volume and a multitude of measurable signals. For example, in materials science or geosciences, elemental composition, grain orientation, and size are useful when coregistered to the grain structure [5]. These data would be obtained using integrated EBSD and energy-dispersive spectroscopy (EDS) detectors (see Table I and Fig. 2). By coupling a FIB with an SEM in one instrument, many inferences are possible from the same sample; thus, multimodal inference is relatively straightforward [6].

Demonstrating a multimodal multiscale workflow at the nanoscale, the authors collected 3-D volumes from a carbonate shale core showing extensive porosity filled with organic material (see Fig. 3). Data were milled and imaged with a Thermo Scientific Helios G4 PFIB DualBeam using Auto Slice and View software. To demonstrate the flexibility of PFIB milling, data were collected at three scales: 300 25 nm slices at 27 nm^2 resolution, 194 50 nm slices at 54 nm^2 resolution, and 296 100 nm^2 slices at 107 nm resolution. Slices took 3.4, 4.4, and 6.5 min per slice to acquire at each resolution, respectively. For porosity analyses, these volumes were merged and resampled to

Table 1. Electron microscopy abbreviations.

Abbreviation	Technology
ABS	Angular backscatter
AFM	Atomic force microscopy
APT	Atom probe tomography
AES	Auger electron spectroscopy
BSE/TLD-BSE	Back-scattered electrons / through the lens detector
BIB/BIB-SST	Broad ion beam serial section tomography
CL	Cathodoluminescence
CBS	Concentric backscatter
CT/CBCT	X-ray computed tomography
EBSD	Electron backscatter diffraction
EELS	Electron energy loss spectroscopy
EDS/EDX	Energy-dispersive X-ray spectroscopy
EMP/EPMA	Electron probe microanalysis
FIB/PFIB	Focused ion beam
SEM/ETD	Scanning electron microscopy
STEM	Scanning transmission electron microscope
SIMS	Secondary ion mass spectrometry
TEM	Transmission electron microscopy

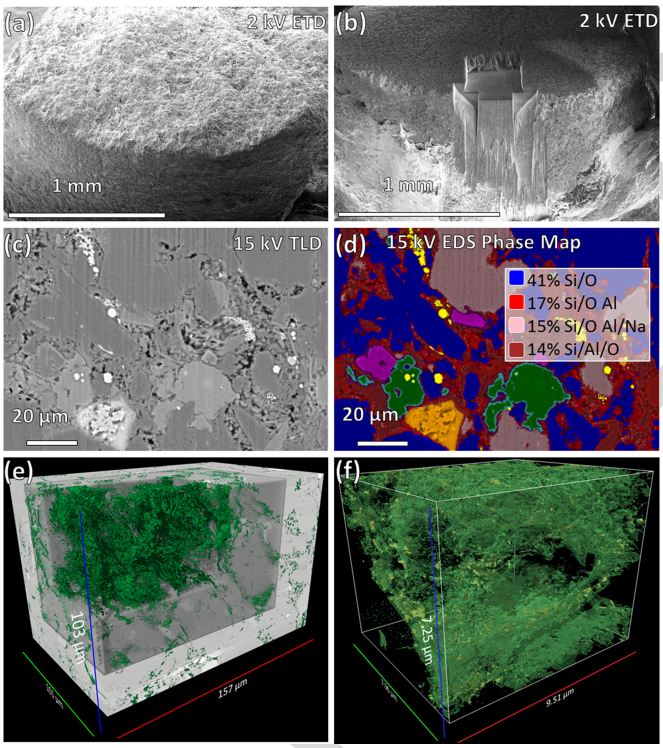

Fig. 3. Everhart–Thornley detector (ETD) SEM of shale carbonate "S51" (a) as received and (b) after manual polishing and bulk milling for site selection. Using a Helios G4 PFIB, slice zero was imaged at 15 kV (c) using the through-the-lens detector (TLD) in BSE mode and (d) mapped by energy dispersive X-ray spectroscopy (EDS) with a 0.267 μm^2 pixel size. The four most prevalent minerals are identified in EDS phase map (d). A PFIB can mill and serially scan samples considered large and dense by FIB standards. This is demonstrated in (e), where the PFIB milled a large portion of S51 at 107 nm^2 resolution and calculated the combined organic matter and porosity (in green) to be 2.80%. (f) PFIB could also resolve porosity from organic matter at 5 nm^3 resolution. In this smaller sample, the organic matter (in green) was 9.75%, and the porosity (in yellow) was 0.340%.

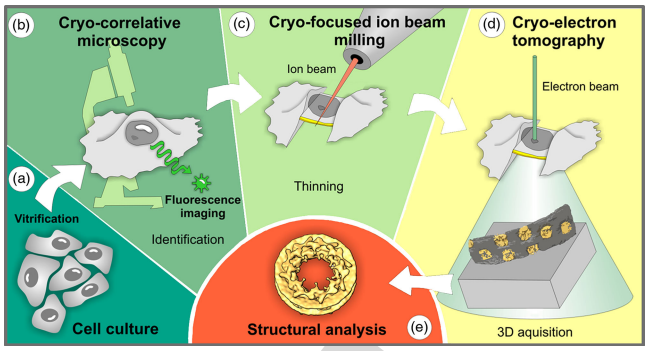

Fig. 4. Cryo-electron tomography workflow with CLEM. (a) Samples deposited on TEM grids are rapidly frozen in vitreous ice to avoid damage caused by crystallization. (b) Cells containing fluorescently labeled proteins are identified in a light microscope in a cryo environment. (c) Labeled cells are relocated to an FIB/SEM that then creates a thin lamella for TEM analysis by milling away material above and below the region of interest. (d) The lamella is transferred to a TEM, which acquires a tomographic image series. (e) Structural analysis is conducted, generating high-resolution 3-D models by a process termed subtomogram averaging and classification.

107.42 × 107.42 × 100 nm voxels in PerGeos. Nominal 100 nm^2 resolution resolved 2.80% porosity, but organic matter and porosity were not always clearly distinguished. Thus, an additional volume was collected at 5 nm^3. At this resolution, porosity resolved from organic matter: 0.34% porosity and 9.75% organic matter (see Fig. 3). EDS phase mapping on the first slice of the large volume at 15 kV was also performed. The EDS mapping and two-resolution PFIB volumes revealed a very tight porosity matrix mostly present at the boundaries of silica and alumina grains.

C. CLEM in a Cryo Environment

In recent years, single particle cryo-EM has emerged as a mainstream structural biology technique that can determine the 3-D structure of proteins and protein complexes at near-atomic resolution [7], [8]. However, single particle cryo-EM is limited to highly purified and isolated proteins that are averaged to determine their 3-D structure and lacks a connection to the cellular context. Cryo-electron tomography instead visualizes proteins within their functional cellular environments. This allows observing their relationships and interactions with other cellular components [9], [10].

As cells are typically on the micron scale and proteins of interest are on the nanometer scale, the target site within the cell must be first localized [11]. Localization of the target region can be done with correlative light and electron microscopy (CLEM; Fig. 4(a)–(c)). In CLEM, samples are first inspected under a fluorescent microscope on a grid with known coordinates. The vitrified sample is then transferred to an FIB–SEM. Here, the superimposition of the cryo-light microscope image with the scanning electron image acquired by the FIB–SEM permits navigation to the features of interest [12].

Protein-scale resolution tomography can be obtained using a TEM, but many cells are too thick for this. Therefore, cells are vitrified or rapidly frozen at −196 °C to avoid damage caused by crystallization and then thinned to 150–300 nm with cryo-FIB prior to imaging in a cryo-TEM [13], [14]. After the milling step, the thinned

samples are transferred to the cryo-TEM, where the actual tomographic image acquisition takes place. From the 3-D tomographic volume, higher resolution structures of particles (i.e., proteins or protein complexes) can be obtained by averaging out noise in a computer-aided process termed subtomogram averaging and classification [15]. Such cryo-CLEM workflows (see Fig. 4) have been used to investigate the structure of inclusions bodies, formed by polyglutamine (polyQ)-expanded huntingtin exon inside primary neuronal mouse and HeLa cells [16]. Additionally, a second study investigated a different type of poly-Gly-Ala peptide related to frontotemporal dementia and amyotrophic lateral sclerosis [17]. Overall, cryo-CLEM allows for labeling features using the biochemistry of fluorescent tagging.

III. CONCLUSION

Multiscale microscopy is often necessary, as it is too expensive, timely, or challenging to collect nano-resolution data at scale. Furthermore, by merging microscope modalities, new insights are often possible. The authors are encouraged by recent reports of new multiscale multimodal microscopy workflows: APT and STEM–EDS [18]; FIB, TEM, and SIMS [19]; and BIB and EBSD [20]; among others. Connecting image scales and modalities will require automatic and intuitive data fusion across machines, reliable software for data extrapolation, and experimental designs that respect ease of use and data utility across platforms.

ACKNOWLEDGMENT

The authors thank H. Long for preparing and imaging the carbonate rock and Gwenole Tallec for the digital rock analysis. Additionally, R. Kelley collected PFIB data, and they were analyzed by N. Vito, A. Aghaei, and C. Burt.

REFERENCES

[1] T. L. Burnett *et al.*, "Correlative tomography," *Sci. Rep.*, vol. 4, 2014, Art no. 4711, doi: 10.1038/srep04711.

[2] R. S. Bradley and P. J. Withers, "Correlative multiscale tomography of biological materials," *MRS Bull.*, vol. 41, pp. 549–554, 2016, doi: 10.1557/mrs.2016.137.

[3] E. Maire and P. J. Withers, "Quantitative X-ray tomography," *Int. Mater. Rev.*, vol. 59, pp. 1–43, 2014, doi: 10.1179/1743280413Y.0000000023.

[4] J. Gelb, D. P. Finegan, D. J. L. Brett, and P. R. Shearing, "Multi-scale 3D investigations of a commercial 18650 Li-ion battery with correlative electron- and X-ray microscopy," *J. Power Sources*, vol. 357, pp. 77–86, 2017, doi: 10.1016/j.jpowsour.2017.04.102.

[5] T. L. Burnett *et al.*, "Large volume serial section tomography by Xe plasma FIB dual beam microscopy," *Ultramicroscopy*, vol. 161, pp. 119–129, 2016, doi: 10.1016/j.ultramic.2015.11.001.

[6] B. Winiarski, G. Pyka, and A. Chirazi, "Multiscale correlative tomography provides critical materials characterization of biomedical implants," *Microsc. Microanal.*, vol. 31, pp. S4–S9, 2017.

[7] C. M. Oikonomou and G. J. Jensen, "Cellular electron cryotomography: Toward structural biology *in situ*," *Annu. Rev. Biochem.*, vol. 86, pp. 873–896, 2017, doi: 10.1146/annurev-biochem-061516-044741.

[8] M. Beck and W. Baumeister, "Cryo-electron tomography: Can it reveal the molecular sociology of cells in atomic detail?," *Trends Cell Biol.*, vol. 26, pp. 825–837, 2016, doi: 10.1016/j.tcb.2016.08.006.

[9] S. Asano, B. D. Engel, and W. Baumeister, "*In situ* cryo-electron tomography—A post-reductionist approach to structural biology," *J. Mol. Biol.*, vol. 428, pp. 332–343, 2016, doi: 10.1016/j.jmb.2015.09.030.

[10] M. Schorb *et al.*, "New hardware and workflows for semi-automated correlative cryo-fluorescence and cryo-electron microscopy/tomography," *J. Struct. Biol.*, vol. 197, pp. 83–93, 2017, doi: 10.1016/j.jsb.2016.06.020.

[11] M. Kellner *et al.*, "A combined method for correlative 3D imaging of biological samples from macro to nano scale," *Sci. Rep.*, vol. 6, 2016, Art no. 35606, doi: 10.1038/srep35606.

[12] G. Wolff, C. Hagen, K. Grünewald, and R. Kaufmann, "Towards correlative super-resolution fluorescence and electron cryo-microscopy," *Biol. Cell*, vol. 108, pp. 245–258, 2016, doi: 10.1111/boc.201600008.

[13] A. Rigort, E. Villa, F. J. B. Bäuerlein, B. D. Engel, and J. M. Plitzko, "Integrative approaches for cellular cryo-electron tomography: Correlative imaging and focused ion beam micromachining," in *Methods in Cell Biology*, vol. 111, T. Müller-Reichert and P. Verkade, Eds. New York, NY, USA: Academic, 2012, pp. 259–281, doi: 10.1016/B978-0-12-416026-2.00014-5.

[14] A. Rigort and J. M. Plitzko, "Cryo-focused-ion-beam applications in structural biology," *Arch. Biochem. Biophys.*, vol. 581, pp. 122–130, 2015, doi: 10.1016/j.abb.2015.02.009.

[15] J. A. G. Briggs, "Structural biology *in situ*—The potential of subtomogram averaging," *Current Opinion Struct. Biol.*, vol. 23, pp. 261–267, 2013, doi: 10.1016/j.sbi.2013.02.003.

[16] F. J. B. Bäuerlein *et al.*, "*In situ* architecture and cellular interactions of PolyQ inclusions," *Cell*, vol. 171, pp. 179–187, 2017, doi: 10.1016/j.cell.2017.08.009.

[17] Q. Guo *et al.*, "*In situ* structure of neuronal C9orf72 Poly-GA aggregates reveals proteasome recruitment," *Cell*, vol. 172, pp. 1–10, 2018, doi: 10.1016/j.cell.2017.12.030.

[18] W. Guo *et al.*, "Correlative energy-dispersive X-ray spectroscopic tomography and atom probe tomography of the phase separation in an alnico 8 alloy," *Microsc. Microanal.*, vol. 22, pp. 1251–1260, 2016, doi: 10.1017/S1431927616012496.

[19] L. Yedra, S. Eswara, D. Dowsett, and T. Wirtz, "*In-situ* isotopic analysis at nanoscale using parallel ion electron spectrometry: A powerful new paradigm for correlative microscopy," *Sci. Rep.*, vol. 6, 2016, Art no. 28705, doi: 10.1038/srep28705.

[20] B. Winiarski, A. Gholinia, K. Mingard, M. Gee, G. E. Thompson, and P. J. Withers, "Broad ion beam serial section tomography," *Ultramicroscopy*, vol. 172, pp. 52–64, 2017, doi: 10.1016/j.ultramic.2016.10.014.